Contrib Mineral Petrol (1999) 135: 151–163

Keith Putirka

Clinopyroxene + liquid equilibria to 100 kbar and 2450 K

Received: 28 May 1997 / Accepted: 20 November 1998

Abstract One of the most active issues in igneous petrology is the investigation of mantle melting, and subsequent differentiation. To evaluate alternative hypotheses for melting and differentiation it is essential to accurately predict clinopyroxene compositions in natural systems. Expressions have thus been derived that describe clinopyroxene-melt equilibria, and allow equilibrium clinopyroxene compositions to be calculated. These equations were constructed from least-squares regression analysis of experimental clinopyroxene-liquid pairs. The calibration database included clinopyroxenes synthesized from both natural and synthetic basalt compositions; experimental conditions ranged from 0 to 100 kbar and 1350 to 2450 K. Regression equations were based on thermodynamic functions. Empirical expressions were also derived, since such models yield more precise estimates of clinopyroxene compositions, and may be easily incorporated into existing liquid line-of-descent models. Such equations may be useful for calculation of high pressure liquid fractionation, or for constraining P-T conditions for basalts produced by partial melting of a pyroxene-bearing source. Models of mantle melting often rely on expressions involving simple element ratios. Partition coefficients ($K_d^{cpx/liq}$) for the minor elements, Na and Ti, were thus also calibrated as a function of P, T and composition. $K_{Ti}^{cpx/liq}$, while sensitive to composition was relatively insensitive to P and T. In contrast, $K_{Na}^{cpx/liq}$ increases substantially with increasing P, and exceeded 1 in some experiments. Since oceanic basalts show variations in Na/Ti ratios, the potential exists for partial melting depths to be inferred from $K_{Na}^{cpx/liq}$.

K. Putirka
Lawrence Livermore National Laboratory
L-202, 700 E. Ave.
Livermore, CA, 94550
925 424-2186
e-mail: putirka1@llnl.gov

Editorial responsibility: T.L. Grove

Introduction

The crystallization and partial melting of clinopyroxene has had a significant impact upon Earth differentiation. Many igneous rocks either contain clinopyroxene as a phenocryst phase, or experienced clinopyroxene fractionation during melt extraction. To address problems of planetary differentiation, it is thus essential to reliably model clinopyroxene-liquid equilibria over wide ranges of pressure (P), temperature (T) and liquid composition. Prior studies of clinopyroxene-liquid equilibria have examined 1-atm phase relationships (Nielsen and Drake 1979; Nielsen et al. 1988), and recent efforts have extended these calibrations to pressures of 12–30 kbar (Ariskin et al. 1993; Sack and Ghiorso 1994). However, clinopyroxene compositions are quite sensitive to P, and to examine such issues as komatiite evolution, or the origin of cratonic peridotite, calibrations at much higher P are required. Clinopyroxene-liquid equilibria have thus been calibrated from experimental data that extend to 100 kbar and 2450 K, so that critical geological problems, that span wide ranges of P and T, might be addressed.

Recent calibrations of clinopyroxene + liquid equilibria have focused upon activity modeling, and the prediction of Gibbs free energies (Sack and Ghiorso 1994; Ghiorso and Sack 1995). Such methods are attractive for a variety of reasons. First, when regression models closely adhere to a thermodynamic form, they are more likely to be useful outside the P-T-composition ranges used for calibration. Second, Gibbs free energy models are very general: the relative stabilities of various liquid and solid phase components may be compared, and the models can apply to a wide range of conditions, including partial melting and subsolidus equilibration. Finally, it is conceivable that the regression techniques employed by Ghiorso and Sack (1995) could be used to extract difficult-to-measure thermodynamic quantities, which may be useful for understanding mineral solution behavior. Nevertheless, it is unclear whether models that

predict Gibbs free energies, or other thermodynamic variables, can be inverted to reliably predict phase composition. To contrast with prior efforts, this study uses clinopyroxene components as dependent variables for regression analysis. Linear and non-linear models are developed, and linear models include empirical corrections. These strategies are employed to maximize the precision with which clinopyroxene components may be calculated. This goal is crucial, since to evaluate competing hypotheses for the origin of igneous rocks, equilibrium phase compositions must be reliably determined. Since this approach differs from that of recent calibrations, the models of this study are compared with those from Sack and Ghiorso (1994) and Ariskin et al. (1993), for their ability to predict clinopyroxene compositions.

Model comparisons and regression strategies

An examination of recent calibrations

The goal of this paper is to produce expressions that reliably predict igneous clinopyroxene compositions to conditions approaching 100 kbar, and 2450 K. Since clinopyroxene + liquid equilibria have yet to be calibrated to $P > 30$ kbar, the expressions presented below should be useful for addressing many critical geological problems. As noted above, though, the strategy adopted for this study contrasts to recent calibration efforts (Sack and Ghiorso 1994; Ghiorso and Sack 1995; Ariskin et al. 1993). Since the expressions of Sack and Ghiorso (1994) and Ariskin et al. (1993), might be inverted to obtain clinopyroxene compositions, it is perhaps appropriate to test such models for their ability to predict clinopyroxene compositions. The models are tested by comparing calculated clinopyroxene compositions to those measured from a variety of experimental studies (Figs. 1 and 2).

Clinopyroxene compositions calculated using MELTS (Ghiorso and Sack 1995; Sack and Ghiorso 1994; Fig. 1) and the models of Ariskin et al. (1993; Fig. 2) do not compare favorably to experimental observations. Except for $AlO_{1.5}^{cpx}$, the Ariskin et al. (1993) models do not extrapolate to $P > 50$ kbar, and do not adequately describe the variation of experimental clinopyroxene compositions. For its calibration data, the Sack and Ghiorso (1994) models recover as much as 70% of the variation for the components *DiHd* and *CaTi* (see Pyroxene Components section below). However, the models perform poorly for the components, *EnFs*, *Jd* and *CaTs*, the calculation of which are critical for estimating pressure and temperature (Putirka et al. 1996). Moreover, the Sack and Ghiorso (1994) models do not extrapolate to high pressure (50–100 kbar), and fail to yield sensible results for approximately 25% of the 10–30 kbar test data. When sensible pyroxene compositions are obtained, the models perform poorly for those data that were not included in the regression analysis, recovering 41% of the variation for *DiHd*, and less than 10% of the variation for all other components. These test results illustrate the need to tailor calibration procedures to a model's intended use.

Regression strategies

To improve our ability to estimate clinopyroxene compositions, certain regression strategies were employed. First, to avoid overfitting the calibration data, it is essential that only the least number of parameters needed to describe the variance of the data are used (Jefferys and Berger 1992; Ratkowsky 1990). When this precept is not followed, some model parameters may be supported by only one or a few, perhaps spurious, data, leading to faulty model parameters. Experimental observations might also have inadequate range to provide leverage in the regression analysis. Without sufficient leverage, parameter estimates can be too large – a small degree of experimental error may lead to a significant apparent effect on a dependent variable. Leverage plots were used to insure that model variables were supported by more than one datum, and that sufficient range in the data was available for parameter estimation. In addition, a variety of models were tested to uncover which sets of parameters best describe a broad range of the experimental data. Experimental data were arbitrarily separated into calibration and test data sets. The test data (not used for calibration) allow a means for comparing various models that provide good fits to the calibration data, but use different variables; one model usually outperforms others.

An additional problem in regression analysis concerns the choice of the dependent variable. Solutions to a regression problem are not symmetric, and error is minimized in one direction only. For example, if $Y = f(X)$, we might derive the equation $Y = \alpha + \beta X + \varepsilon$ (where α and β are coefficients derived from regression analysis, and ε is an error term). Such an equation may be satisfactory for predicting Y when X is observed, but can be a very poor predictor of X if the equation were rearranged; to reliably predict X, an independent regression should be performed, with X as the dependent variable. When variables of interest are unfolded from a complex model, estimates may be unreliable. To provide expressions that predict clinopyroxene compositions, clinopyroxene components were used as dependent variables in the regression analysis. Additionally, all models should account for error in the experimental data gathering process (ε). The residual sum of squares (and ε) will always be reduced by addition of variables, but ε should never be less than experimental imprecision. This problem can be avoided when the minimum number of model parameters are regressed (see Ratkowsky 1990; Ryan 1997).

Finally, to reliably estimate clinopyroxene compositions, it is most useful if the regression equation is linear in the regression parameters. Non-linear equations allow for a strict thermodynamic description of clinopyroxene + liquid equilibria, but non-linear regression has

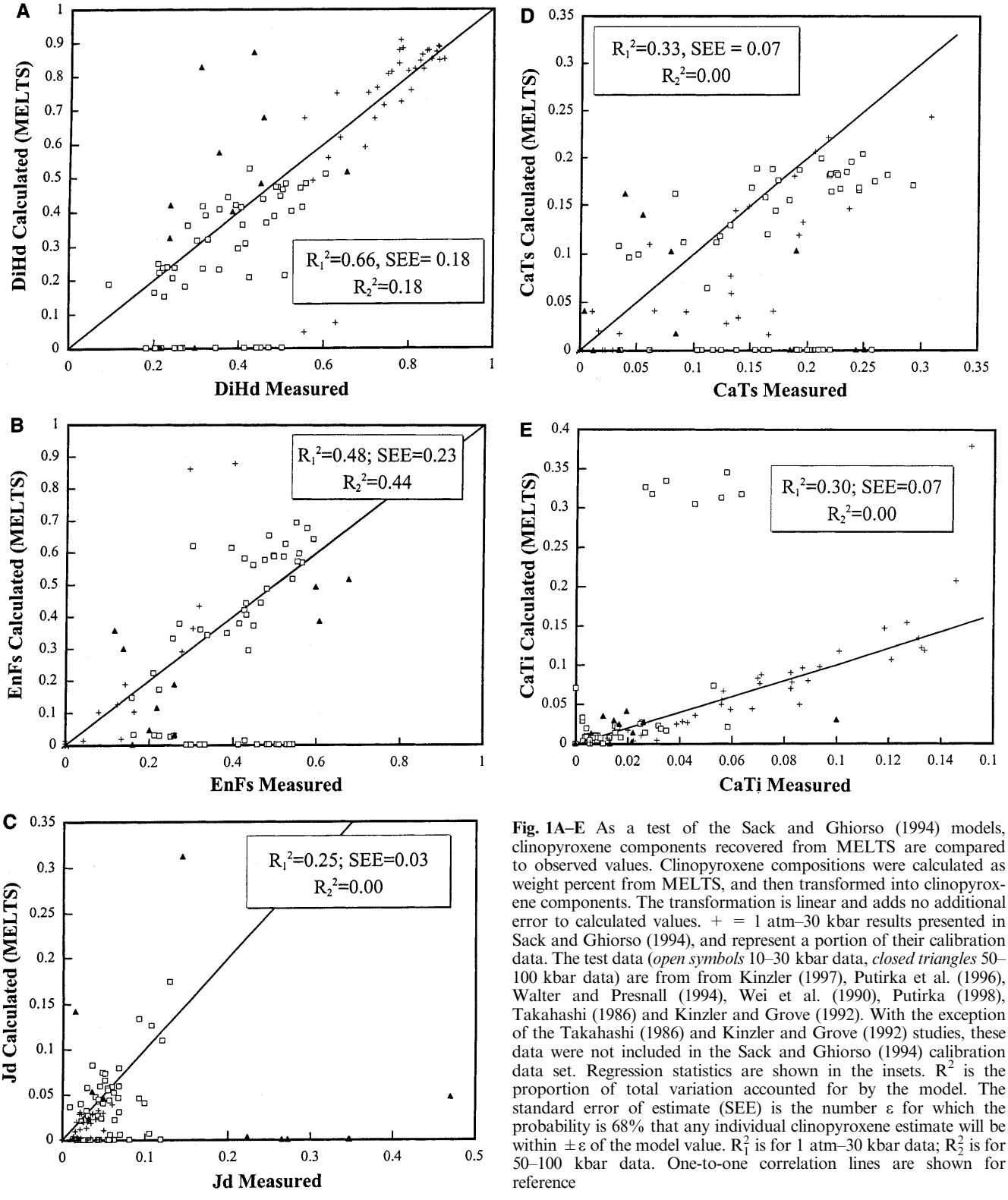

Fig. 1A–E As a test of the Sack and Ghiorso (1994) models, clinopyroxene components recovered from MELTS are compared to observed values. Clinopyroxene compositions were calculated as weight percent from MELTS, and then transformed into clinopyroxene components. The transformation is linear and adds no additional error to calculated values. + = 1 atm–30 kbar results presented in Sack and Ghiorso (1994), and represent a portion of their calibration data. The test data (*open symbols* 10–30 kbar data, *closed triangles* 50–100 kbar data) are from from Kinzler (1997), Putirka et al. (1996), Walter and Presnall (1994), Wei et al. (1990), Putirka (1998), Takahashi (1986) and Kinzler and Grove (1992). With the exception of the Takahashi (1986) and Kinzler and Grove (1992) studies, these data were not included in the Sack and Ghiorso (1994) calibration data set. Regression statistics are shown in the insets. R^2 is the proportion of total variation accounted for by the model. The standard error of estimate (SEE) is the number ε for which the probability is 68% that any individual clinopyroxene estimate will be within ±ε of the model value. R_1^2 is for 1 atm–30 kbar data; R_2^2 is for 50–100 kbar data. One-to-one correlation lines are shown for reference

disadvantages (Ratkowsky 1990). In particular, non-linear regression provides non-unique parameter estimates, and a best fit to calibration data is never ensured. It is thus essential to keep model non-linearity to a minimum. Non-linear regression analysis can be avoided altogether if a regression equation can be made linear, but this strategy may require that some variables take an empirical form. When the form of empirical variables is non-arbitrary, though, it may be possible to build models that feature improved precision, and that are

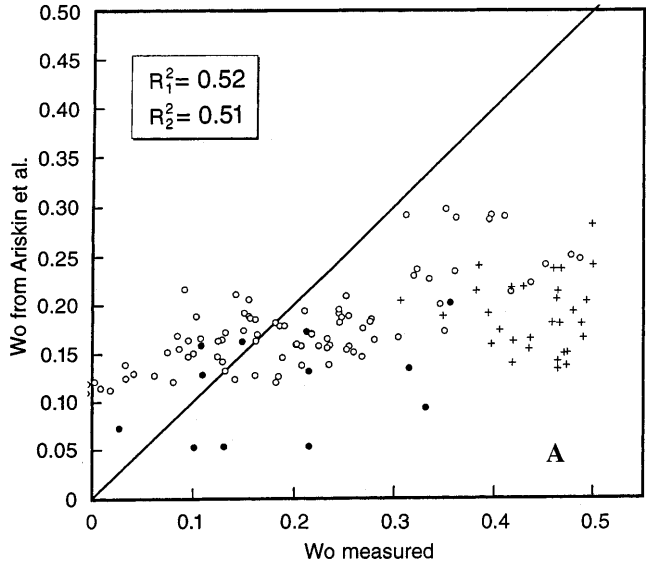

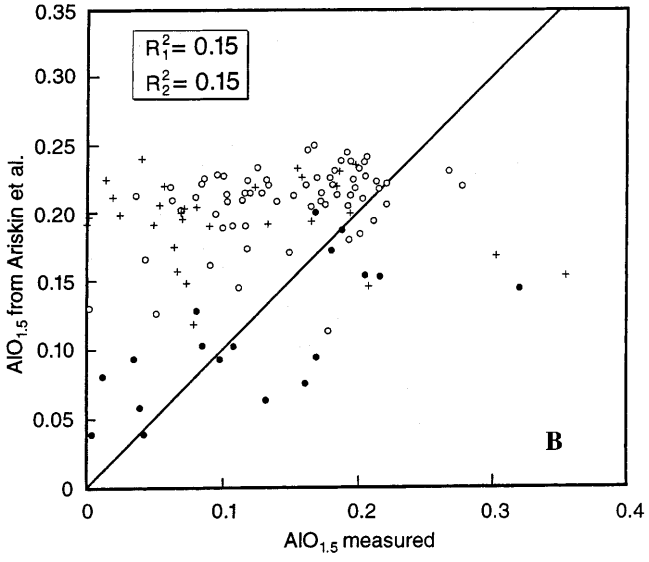

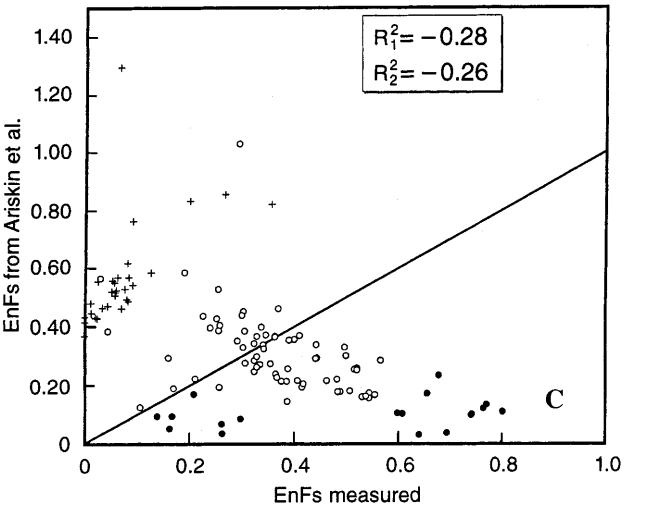

◀

Fig. 2A–C Clinopyroxene components calculated using the Ariskin et al. (1993) models are compared to observed values. *Wo* wollastonite, *EnFs* enstatie + ferrosilite, $AlO_{1.5}$ is the cation fraction of Al in clinopyroxene. See Fig. 1 caption for experimental data used for testing, and chart details. The data shown were not used by Ariskin et al. (1993) for calibration

useful as predictive tools. Empirical expressions are thus developed so that linear regression analysis could be performed.

Methods

The approach of this study was similar to that used for analysis of garnet + liquid equilibria (Putirka 1998) and the calibration of pyroxene-liquid thermobarometers (Putirka et al. 1996; see also Nielsen and Drake 1979; Roeder and Emslie 1970); equilibrium constants (K_{eq}) for crystallization equilibria (Table 1) were calibrated against P, T and compositional variables. The experimental data used for analysis (Fig. 3) include bulk compositions that range from nephelinite to komatiite, and experimental pressures that range from 1 atm to 100 kbar. The experimental data were selected based upon several criteria. These criteria include an examination of analytical technique and charge balance for reported clinopyroxene compositions (see Putirka et al. 1996), as well as the treatment of uncertainties on T for experiments performed in the multianvil apparatus (Putirka 1998).

Pyroxene components

In order to calculate equilibrium constants, activity models for pyroxene and liquid components must be assumed. In this study liquid components were calculated as cation fractions. Non-idealities were treated as in Putirka et al. (1996), where ideal and non-ideal components of the equilibrium constant were separated using the definition of the activity coefficient ($a_i^\alpha = X_i^\alpha \lambda_i^\alpha$, where a_i^α = activity of i in phase α, X_i^α is the mole fraction of i in α, and λ_i^α is the activity coefficient). Pyroxene components were calculated using a procedure that was slightly modified from Putirka et al. (1996). As in Putirka et al. (1996), pyroxenes are calculated on a six oxygen basis, and the charge balance equation of Lindsley (1980) is applied to all experimental pyroxenes. Also, as in Putirka et al. (1996), only Fe^{2+} and Mg are used for calculation of *EnFs* (enstatite + ferrosilite) and *DiHd* (diopside + hedenbergite) components. A Cr-bearing component, *Cr-CaTs* ($CaCr_2SiO_6$ = Cr/2) is added to the calculation scheme. If Ca^{cpx} is insufficient to form *Cr-CaTs*, Ca-Tschermak (*CaTs*; $CaAl^{VI}Al^{IV}SiO_6$) and *CaTi* ($CaTi_2AlO^6$) components, then Fm^{cpx} ($=FeO^{cpx}+MgO^{cpx}$) is used to form the components *Fm-CaTs* ($FmAl^{VI}Al^{IV}SiO_6$) and *FmTi* ($FmTiAl_2O_6$). In such cases *DiHd* is zero, and *EnFs* is formed from the remaining Fm^{cpx}. Pyroxene components calculated by this

Table 1 Equilibria[a]

Pyroxene + liquid equilibria used for calibration	
$CaO^{liq} + FmO^{liq} + 2SiO_2^{liq} = CaFmSi_2O_6^{pyx}$	(1.1)
$2SiO_2^{pyx} + 2FmO^{liq} = Fm_2Si_2O_6^{pyx}$	(1.2)
$Mg^{pyx} + FeO^{liq} = Fe^{pyx} + MgO^{liq}$	(1.3)
$CaO^{liq} + 2AlO_{3/2}^{liq} + SiO_2^{liq} = CaAl_2SiO_6^{pyx}$	(1.4)
$NaO^{liq} + AlO_{3/2}^{liq} + 2SiO_2^{liq} = NaAlSi_2O_6^{pyx}$	(1.5)
$CaO^{liq} + 2AlO_{3/2}^{liq} + TiO_2^{liq} = CaAl_2TiO_6^{pyx}$	(1.6)
$CaO^{liq} + 2CrO_{3/2}^{liq} + SiO_2^{liq} = CaCr_2SiO_6^{pyx}$	(1.7)

[a] Terms such as $CaFmSi_2O_6^{pyx}$ indicate the mole fraction of $CaFmSi_2O_6$ in clinopyroxene. The symbol Fm refers to total (FeO + MgO). Terms such as Mg^{liq} refer to the cation fraction of the indicated element in the liquid

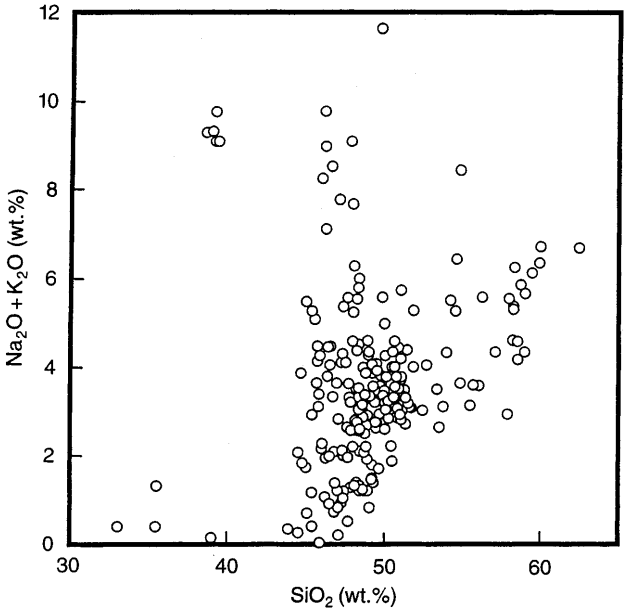

Fig. 3 Weight percent SiO_2 is compared to weight percent $Na_2O + K_2O$, for liquid compositions in calibration and test data sets. Predictions of clinopyroxene compositions using the models of Table 3 should be most reliable for natural liquids that are within this compositional range. The experimental data are from: Bartels et al. (1991), Bender et al. (1984), Blundy et al. (1995), Elthon and Scarfe (1984), Falloon and Green (1987), Grove et al. (1992), Grove and Juster (1989), Hack et al. (1994), Juster et al. (1989), Kinzler and Grove (1992), Longhi (1995), Putirka et al. (1996), Putirka (1998), Sack et al. (1987), Takahashi (1986), Tormey et al. (1987), Walter and Presnall (1994), Wei et al. (1990), Yasuda and Fujii (1994)

scheme should be very close to unity; components are normalized to unity for the regression analysis.

Longhi and Bertka (1996) have shown that clinopyroxenes with very low Ca-contents may occur on the mantle solidus, in equilibrium with orthopyroxenes. Such low Ca-contents result from the shape of the orthopyroxene-clinopyroxene solvus at high T (Lindsley 1980). All reported clinopyroxene compositions that yielded a *DiHd* component >0 were thus used for calibration of the clinopyroxene saturation surface. Using the normative procedure outlined above, pyroxenes had an average X^{pyx}_{DiHd} of 0.46 with a range of $0.1 < X^{pyx}_{DiHD} < 0.86$, while the average X^{pyx}_{EnFs} was 0.32 and the range was $0.03 < X^{pyx}_{EnFs} < 0.74$.

Regression models

In many geological studies P and T are the variables of interest, and various petrologic devices are employed for their determination. For clinopyroxenes, methods currently exist for estimating P and T when pyroxene and liquid compositions are available (Putirka et al. 1996). For many critical geological problems, though, it is essential to predict pyroxene compositions when P, T and a liquid composition are given.

To predict mineral components, linear expressions can be obtained when crystallization equilibria are calibrated, and when mineral components approach ideal solutions (Putirka 1998). For clinopyroxenes, however, mixing between components such as *DiHd* and *EnFs*, is strongly non-ideal (Grover and Orville 1969; Grover 1980; see also Sack and Ghiorso 1994), and equations describing crystallization equilibria become non-linear. To derive linear regression equations, empirical parameters must be employed. To illustrate how empirical parameters are obtained, a non-linear expression is given below. Equation 1 is a simplified description of the crystallization of clinopyroxene component i, which interacts with component j. A symmetric Margules model is used to describe non-ideal interactions (Nordstrom and Munoz 1986),

$$\ln[X_i^{cpx}] = \frac{\Delta S_{fus}}{R} - \frac{\Delta H_{fus} + \Delta C_p(T - T_m)}{RT} + \frac{\Delta C_p}{R}\ln\frac{T}{T_m} - \frac{(P - P_0)\Delta V_{fus}}{RT} + \ln[X_i^{liq}] + W_G^{i-j}\frac{X_i^{cpx}X_j^{cpx}}{RT} + \lambda^{i-j}\frac{X_i^{liq}X_j^{liq}}{RT}. \quad (1)$$

Terms such as X_i^{liq} and X_i^{cpx} represent the mole fractions of component i in liquid and clinopyroxene respectively. R is the gas constant, and T_m is the melting temperature of X_i^{cpx} at reference pressure P_0. Quantities such as $\Delta S_{fus}, \Delta H_{fus}, \Delta V_{fus}$ and ΔC_p, respectively refer to the entropy, enthalpy, volume and heat capacity differences of products and reactants. W_G^{i-j} is a Margules interaction parameter for pyroxene components i and j. The term λ^{i-j} is an interaction parameter for liquid components X_i^{liq} and X_j^{liq}. For regression analysis, the input data are experimental observations of P, T and X_i; quantities such as $\Delta S_{fus}, \Delta H_{fus}, \Delta V_{fus}, \Delta C_p, W_G^{i-j}$ and λ^{i-j} are obtained from regression analysis. In Eq. 1, the variable of interest, X_i^{cpx}, cannot be isolated, and non-linear regression analysis is required.

To obtain a linear expression, the variable of interest, X_i^{cpx}, may be dropped from the term $[W_G^{i-j}X_i^{cpx}, X_j^{cpx}]/R\mathrm{T}$ and replaced with the term $[\beta X_j^{cpx}]/R\mathrm{T}$, where β is an empirical parameter. While the thermodynamic interpretation of β is less clear compared to W_G^{i-j}, this substitution retains the expected X_j^{cpx}/T dependency. Non-ideal, asymmetric solutions can be similarly approximated using empirical variables of the form $[\beta(X_i^{cpx})^2]/R\mathrm{T}$. Such substitutions yield regression problems that are linear, and the drawbacks of non-linear regression are avoided. The resulting empirical expressions have the additional advantage that they are easily evaluated, and may be incorporated into existing geologic models, such as liquid-line-of-descent spreadsheets or programs.

Results

The linear empirical models outperform models derived by non-linear regression methods (Tables 2 and 3), even when empirical models contain fewer adjustable parameters. In addition to reproducing the calibration data, the empirical models successfully predict clinopyroxene compositions from the test data. Some test data are hi-lighted in Figs. 4 and 5; these experiments are different from the calibration data either because of differences in bulk composition (Longhi and Pan 1988; Sack and Ghiorso 1994; Sack et al. 1987; Longhi 1996) or because of unique experimental conditions (Baker and Stolper 1994; Robinson et al. 1998).

In general, each of the equations in Tables 2 and 3 produce residuals that are uncorrelated with P, T and liquid or mineral composition. This lack of correlation indicates that the models account for the variation of clinopyroxene compositions, within the limits of experimental error. Since high-pressure experiments are not controlled for oxygen fugacity (f_{O_2}), this variable was not used for modeling purposes. Residuals for the models presented in Table 3, though, are not correlated with f_{O_2} for the 1-atm data where f_{O_2} was controlled. The model residuals (see insets to Figs. 4 and 5) likely result from the sum of errors of measurement of P, T

Table 2 Non-linear expressions for *DiHd*, *EnFs* and *CaTs* components[a]

Results from non-linear regression	R^2(SEE)	Equation
$\ln[DiHd^{cpx}] = -6.07 + \frac{13611}{T} + 4.88\ln\left(\frac{T}{1670}\right) + 0.74\ln[Ca^{liq}Fm^{liq}(Si^{liq})^2] - 2.96\times10^3\left[\frac{EnFs^{cpx}DiHd^{cpx}}{T}\right] - 0.74[Fm^{liq}]$	0.82(0.07)	(2.1)
$\ln[EnFs^{cpx}] = -1.68 + \frac{17000}{T} + 9.2\ln\left(\frac{T}{1670}\right) + 0.02\frac{P}{T} - 6.4\times10^{-7}\frac{P^2}{T} + 0.46\ln[(Fm^{liq})^2(Si^{liq})^2] - 2.96\times10^3\left[\frac{(EnFs^{cpx})DiHd^{cpx}}{T}\right] + 0.96\ln[Mg^{liq}] + 4.8\ln[Si^{liq}] - 5.3\times10^4\frac{SiCa^{liq}}{T}$	0.63(0.13)	(2.2)
$\ln[CaTs^{cpx}] = -7.7 + \frac{10000}{T} + 0.23\frac{P}{T} - 1.0\times10^{-6}\frac{P^2}{T} + 1.81\ln[(Fm^{liq})^2(Si^{liq})^2] - 2.0\times10^3\left[\frac{(CaTs^{cpx})DiHd^{cpx}}{T}\right] - 2.4\ln[Ca^{liq}] - 5.5\ln[Si^{liq}] - 4.9\times10^4\frac{SiNa^{liq}}{T}$	0.60(0.05)	(2.3)

[a] T is in Kelvins and P is in bars. *DiHd*, *EnFs* and *CaTs* refer to the mole fractions in clinopyroxene of Diopside + Hedenbergite and Enstatite + Ferrosilite, and Ca-Tschermak components respectively. The symbol *Fm* refers to total (FeO + MgO). Terms such as Mg^{liq} refer to the cation fraction of the indicated element in the superscripted phase. $SiCa^{liq}$ represents the product of liquid cation fractions of Si and Ca. A reference temperature of 1670 K was used in the regression equations since this temperature is close to the reported metastable melting point of pure diopside at 1 atm (Richet and Bottinga 1986). R^2 values are given, along with SEE values, in parentheses

and composition, and any error associated with a lack of attainment of equilibrium.

For the clinopyroxene components *DiHd*, *EnFs*, *CaTs* and *CaTi*, it was necessary to account for non-ideal mixing. In all cases, only mixing between the component of interest and either *DiHd*, or *EnFs* was required to describe the data. Crystallization equilibria for *DiHd*, *EnFs*, and *CaTs* were thus derived from global non-linear regression (Table 2). The non-linear models use a symmetrical Margules parameterization for pyroxene mixing; asymmetric models were also tested, but yielded little or no statistical improvement, and coefficients compared unfavorably to known thermodynamic quantities.

For jadeite (*Jd*) the incorporation of excess mixing energy terms yielded no improvement in the model. This may reflect the high *T*s of the calibration data, compared to the low T of the consolute point for the *Jd*-Augite solvus (700 °C; Buseck et al. 1980). At such high T the magnitude of non-ideal mixing contributions decreases and solutions may approach ideal behavior (Navrotsky 1981). This does not imply that non-ideal contributions to the equilibrium are non-existent, only that the energetics of mixing cannot be clearly resolved within the experimental error of the calibration data. Non-linear regression for *Jd* was thus unnecessary, and only linear regression results are presented (Table 3).

Solution of Ti and Cr in clinopyroxene were modeled using the components *CaTi* ($CaTiAl_2O_6$) (see Gee and Sack 1988) and *Cr-CaTs* ($CaCr_2SiO_6$) respectively. Equation numbers quoted in this and the next paragraph are from Tables 1–3. These components, and *CaTs* were characterized by greater variance, compared to other clinopyroxene components. In the case of *Cr-CaTs* little systematic variation was observed, and the K_{eq} for Eq. 1.7 was modeled as a constant using a global average (Eq. 3.7). For the *CaTi* and *CaTs* components, global regressions provided the best fits compared to attempts to split data into test and regression sets. The model for *CaTs* (Eq. 3.4) describes much of the high P variation, but considerable residual variance was evident in the 1 atm data set. Such variance was not correlated with T, f_{O_2}, or compositional variables, and might be due to experimental error, although it is uncertain why experimental error for 1 atm experiments should be greater for this component. Eq. 3.4 is nevertheless successful at detecting significant changes in *CaTs* over substantial ranges of P and T.

The Fe content of pyroxenes was modeled using an Fe-Mg exchange equilibrium, $K_D^{Fe-Mg} = Fe^{pyx}Mg^{liq}/Mg^{pyx}Fe^{liq}$, analogous to that used by Roeder and Emslie (1970) for olivines. The compositional terms in Eq. 3.3 are similar to compositional dependencies discovered for the olivine-liquid K_D^{Fe-Mg} by Gee and Sack (1988) and Langmuir et al. (1992). Since f_{O_2} was not controlled for the high pressure experiments, the Fe-Mg exchange K_D was calibrated only for experiments run in graphite capsules, and yielding clinopyroxenes with negligible Fe^{+3} (few such clinopyroxenes required Fe^{3+} based on the charge balance constraints of Lindsley 1983). Since Eq. 3.3 was calibrated over a restricted range of f_{O_2} conditions, Eq. 3.3 will probably not extrapolate to clinopyroxenes crystallized under oxidized conditions.

Minor-element partition coefficients for pyroxene-liquid

Simple partition coefficients (K_d) are often used in petrogenetic modeling. Models based on experimentally calibrated K_d provide a convenient way to estimate the conditions of igneous processes, such as mantle melting,

Table 3 Linear equations[a]

Regression results for linear regression equations

$$\ln[DiHd^{pyx}] = -9.8 + 0.24\ln[Ca^{liq}Fm^{liq}(Si^{liq})^2] + \frac{17558}{T} + 8.7\ln\left(\frac{T}{1670}\right) - 4.61\times10^3\left[\frac{(EnFs^{cpx})^2}{T}\right] \quad (3.1a)$$

$$\ln[DiHd^{cpx}] = -8.65 + 0.80\ln[Ca^{liq}Fm^{liq}(Si^{liq})^2] + \frac{17419}{T} + 0.02\frac{P}{T} + 6.2\ln\left(\frac{T}{1670}\right) - 0.83\ln[Fm^{liq}] \quad (3.1b)$$

$$\ln[EnFs^{pyx}] = -6.96 + \frac{18438}{T} + 8.0\ln\left(\frac{T}{1670}\right) + 0.66\ln[(Fm^{liq})^2(Si^{liq})^2] - 5.1\times10^3\left[\frac{(DiHd^{pyx})^2}{T}\right] + 1.81\ln[Si^{liq}]. \quad (3.2)$$

$$\ln\left(\frac{Fe^{pyx}Mg^{liq}}{Mg^{pyx}Fe^{liq}}\right) = 31.8 - 36.8[Si^{liq}] - 4.76[Na^{liq}] + 17.0\ln[Si^{liq}] - \frac{3879}{T} - 0.014\frac{P}{T}. \quad (3.3)$$

$$\ln[CaTs^{cpx}] = 2.58 + 0.12\frac{P}{T} - 9\times10^{-7}\frac{P^2}{T} + 0.78\ln[Ca^{liq}(Al^{liq})^2Si^{liq}] - 4.3\times10^3\frac{[(DiHd^{cpx})^2]}{T} \quad (3.4)$$

$$\ln[Jd^{pyx}] = -1.06 + 0.13\frac{P}{T} - 6\times10^{-7}\frac{P^2}{T} + 1.02\ln[Na^{liq}Al^{liq}(Si^{liq})^2] - 0.80\ln[Al^{liq}] - 2.2\ln[Si^{liq}] \quad (3.5)$$

$$\ln[CaTi^{pyx}] = 5.1 + 0.52\ln[Ca^{liq}Ti^{liq}(Al^{liq})^2] + 2.04\times10^3\left[\frac{(DiHd^{cpx})^2}{T}\right] - 6.2[Si^{liq}] + 42.5[NaAl^{liq}] - 45.1[FmAl^{liq}] \quad (3.6)$$

$$\ln\left[\frac{CaCr_2SiO_6}{Ca^{liq}(Cr^{liq})^2Si^{liq}}\right] = 12.8 \pm 1.8 \quad (3.7)$$

$$\frac{10^4}{T(K)^{CpxSat}} = 3.12 - 2.59\times10^{-2}P(kbar) - 0.37\ln[Mg\#^{liq}] + 0.47\ln[Ca^{liq}Fm^{liq}(Si^{liq})^2] - 0.78\ln[(Fm^{liq})^2(Si^{liq})^2] - 0.34\ln[Ca^{liq}(Al^{liq})^2Si^{liq}] \quad (3.8)$$

[a] Terms as in Tables 1 and 2. T^{CpxSat} = temperature of clinopyroxene saturation

where equilibrium solid and liquid compositions are not known (Langmuir et al. 1992). For this reason, minor element partition coefficients were calibrated.

Prior calibrations of $K_{\mathrm{Na}}^{cpx/liq}$ (Langmuir et al. 1992; Blundy et al. 1995) and $K_{\mathrm{Ti}}^{cpx/liq}$ (Ray et al. 1983; Langmuir et al. 1992; Forsythe et al. 1994) have been based on relatively low pressure experiments, compared to the data used for this study. These earlier formulations underestimate the $K_{Na}^{cpx/liq}$ and $K_{Ti}^{cpx/liq}$ observed in experiments performed at higher pressure (> 30 kbar). Since high pressure pyroxene-liquid partitioning is important for understanding mantle melting, new regressions for $K_{Na}^{cpx/liq}$ and $K_{Ti}^{cpx/liq}$ were performed. Both $K_{Na}^{cpx/liq}$ and $K_{Ti}^{cpx/liq}$ were regressed using liquid compositions as independent variables. Each of the following equations were derived from global regression analysis. The resulting functions are,

$$\ln\left(\frac{Na^{cpx}}{Na^{liq}}\right) = -2.17 + 0.12\left(\frac{P(bars)}{T(K)}\right) - 5.8\times10^{-7}\left(\frac{P(bars)^2}{T(K)}\right) - 0.6\left(Mg\#^{liq}\right) \quad (2)$$

and

$$\ln\left(\frac{Ti^{cpx}}{Ti^{liq}}\right) = 0.22 + 8.01Al^{liq} - 5.53Si^{liq} - 9.46Fm^{liq} - 0.40\ln\left[NaAl^{liq}\right] \quad (3)$$

Calculated values for $K_{Na}^{cpx/liq}$ and $K_{Ti}^{cpx/liq}$ using Eqs. 2 and 3 are compared to measured quantities for the

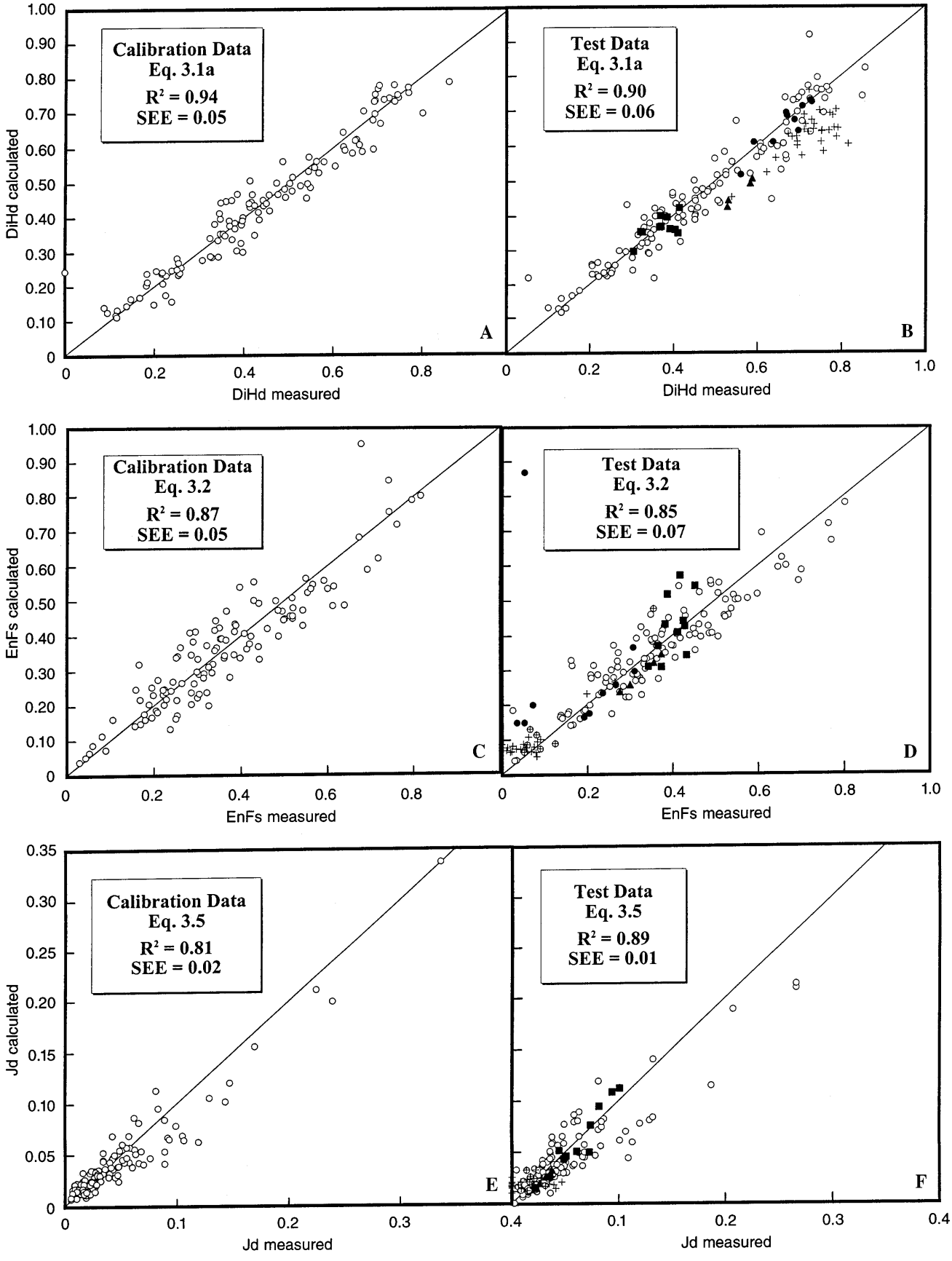
Calibration Data
Eq. 3.1a
R² = 0.94
SEE = 0.05
Test Data
Eq. 3.1a
R² = 0.90
SEE = 0.06
DiHd calculated
DiHd measured
A
B
Calibration Data
Eq. 3.2
R² = 0.87
SEE = 0.05
Test Data
Eq. 3.2
R² = 0.85
SEE = 0.07
EnFs calculated
EnFs measured
C
D
Calibration Data
Eq. 3.5
R² = 0.81
SEE = 0.02
Test Data
Eq. 3.5
R² = 0.89
SEE = 0.01
Jd calculated
Jd measured
E
F

◀

Fig. 4A–F Calculated clinopyroxene compositions are compared to observed values for models (in Table 3) that were divided into Test and Calibration sets. Equation numbers (Table 3), data sets, and statistics (see Fig. 1 caption for explanation) are shown in insets, and one-to-one correlation lines are shown for reference. The figures on the left show recovery of calibrated clinopyroxene compositions; figures on the right show estimates for data not used for calibration. Several test data sets are hi-lighted: high Fe data from Longhi and Pan (1988) and high Fe-Ti data from Longhi (1996) and Delano (1980) (*filled circles*), alkalic basalts from Sack and Ghiorso (1994) and some alkalic basalts from Sack et al. (1997) (*pluses*), low melt fraction experiments from Baker and Stolper (1994) (*filled triangles*), and Robinson et al. (1998) (*filled squares*). The test data address issues of interpolation and extrapolation for the empirical models (see text)

partition coefficients in Figs. 6A and 6B respectively. As is evident from the compositional corrections to Eq. 3, the Al^{liq}-sensitivity of $K_{Ti}^{cpx/liq}$ noted by Forsythe et al. (1994) and Hack et al. (1994), was also evident in the present data set (see also Skulski et al. 1994, Adam and Green 1994, and Hauri et al. 1994).

Since some mantle melting models calculate liquid compositions from mineral/melt partition coefficients (Langmuir et al. 1992), the partition coefficient for Na was also calibrated without additional liquid composition terms, yielding,

$$\ln\left(\frac{Na^{cpx}}{Na^{liq}}\right) = -2.48 + 0.11\left(\frac{P(bars)}{T(K)}\right) - 5\times10^{-7}\left(\frac{P(bars)^2}{T(K)}\right) \quad (4)$$

Recovery of $K_{Na}^{cpx/liq}$ using Eq. 4 is shown in Fig. 6C. In contrast to $K_{Na}^{cpx/liq}$, the $1/T$ term appearing in (Eq. 3) for $K_{Ti}^{cpx/liq}$ was only statistically significant after compositional variation had been accounted for, with such terms as $NaAl^{liq}$. Since variations in $K_{Ti}^{cpx/liq}$ due to temperature are small compared to compositional variations, a compositional independent $K_{Ti}^{cpx/liq}$ was modeled as a constant,

$$\frac{Ti^{pyx}}{Ti^{liq}} = 0.47 \pm 0.28. \quad (5)$$

Discussion

The expressions presented in Table 3 reproduce the calibration data, and also successfully predict clinopyroxene compositions from the test data. Since empirical corrections were employed, the test data are of particular importance for determining the reliability of such models. Significantly, the empirical models predict clinopyroxene compositions from a variety of extreme liquid compositions that were not used for regression analysis. For example, the models recover clinopyroxene components from experimental liquids that have very high Fe (Longhi and Pan 1988), and high Fe + Ti (lunar compositions, Longhi 1996; Delano 1980). Liquids from these experiments contain Fe and Ti contents ranging up to 21 and 24 wt% respectively, greatly exceeding those values that are in the calibration data set. In addition, the models successfully predict clinopyroxene components for alkalic samples from Sack et al. (1987) and from Sack and Ghiorso (1994; equilibrated in air). For

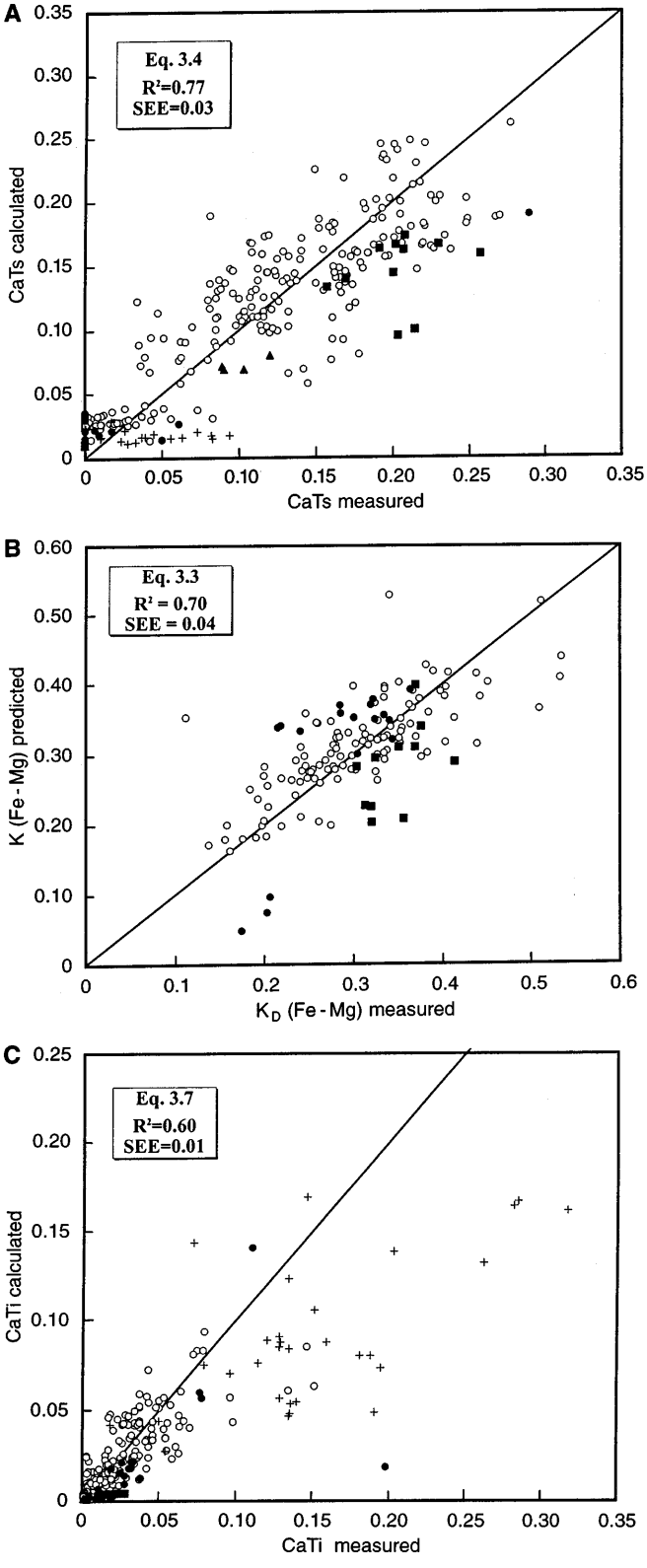

Fig. 5A–C Clinopyroxene compositions recovered from global regression analysis are compared to observed values for models in Table 3. Insets as in Fig. 2

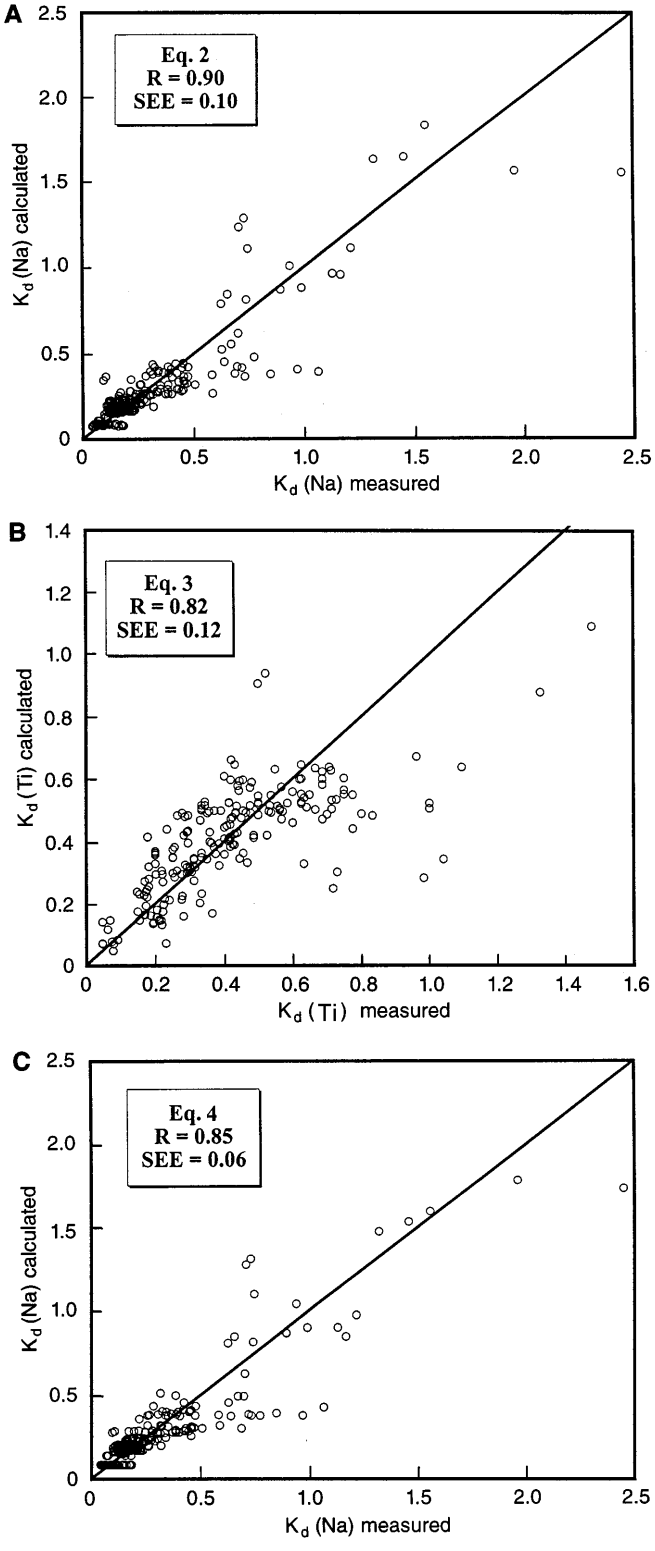

Fig. 6A–C Partition coefficients are recovered for the calibration data, using Eqs. 2, 3, and 4. Insets as in Fig. 2

these data, all components except for *CaTi* are reproduced within model error (the *CaTi* model was not improved when these data were incorporated into the regression analysis). Successful prediction of such extreme compositions indicates that the models may be robust against at least modest departures from the calibration data.

The experiments of Baker and Stolper (1994) and Robinson et al. (1998) provide an additional and interesting set of test data. The data are unique because they cover a specific range of *P-T*-bulk composition space that is not covered by the calibration data. These low melt fraction experiments are important because they closely simulate melting conditions that are likely encountered in Earth's upper mantle. Most importantly, the models of Table 3 successfully predict the Baker and Stolper (1994) and Robinson et al. (1998) clinopyroxene compositions, even though the models were calibrated using high melt fraction experiments (Fig. 3). It is also interesting that Robinson et al. (1998) similarly discovered that the models of Kinzler and Grove (1992; derived from higher melt fraction experiments) successfully predict their low melt fraction liquid compositions.

It appears that high melt fraction experiments can be safely extrapolated to low-melt fraction conditions. It is perhaps significant, though, that the Baker and Stolper (1994) and Robinson et al. (1998) experiments are only extreme with respect to melt fraction. Compared to the calibration data, these experiments are not extreme in their *P-T* conditions, nor are they extreme in regard to the liquid and clinopyroxene compositions that are produced. Thus, even though the precise coincidence of *P-T*-bulk composition space is not covered by the calibration data of this study, no extrapolation in *P-T-X* space is required of the clinopyroxene models (Table 3). The success of the clinopyroxene and Kinzler and Grove (1992) models appear to indicate that (1) the low and high melt fraction experiments are internally consistent and (2) for purposes of geologic interpretation, it may not be necessary to experimentally reproduce a specific set of P-T-X_i conditions, so long as the conditions of interest may be interpolated from an appropriately broad set of experimental observations.

An additional test of the models concerns the thermodynamic quantities obtained from the regression coefficients (Tables 2, 3; Table 4). Coefficients for *P-T* terms yield parameters (Table 2) that match well with values derived from calorimetry, except for ΔS_c values for *CaTi* and *CaTs* (Navrotsky 1981; Richet and Bottinga 1986; Robie et al. 1979; Lange and Carmichael 1987; for diopside $\Delta H_c = -138$ kJ/mol; $\Delta S_c = -83$ J/K*mol; $\Delta C_p = -92$ J/K*mol; $\Delta\beta = -2 \times 10^{-5}$/b, where the subscript '*c*' refers to the crystallization equilibrium). Margules interaction parameters for clinopyroxene components are also in the range estimated by Ottonello (1992). Melt interaction energies, though, greatly exceed values anticipated from calorimetry (Navrotsky et al. 1989). This disagreement for melt interaction energies is also a feature of the Ghiorso and Sack (1995) model. Such error almost certainly stems, in part, from application of incorrect activity models. There is also the likelihood that mixing energies vary

Table 4 Thermodynamic quantities from regression coefficients[a]

	ΔH_c	ΔS_c	ΔV_c	ΔC_p	$\Delta\beta$	$W_G^{Di\text{-}En}$	$W_G^{Di\text{-}CaTs}$	$W_G^{Si\text{-}Ca}$	$W_G^{Si\text{-}Na}$
Eq. 3.1a	−146	−81	–	−72	–	–	–	–	–
Eq. 3.2	−153	−58	–	−66	–	–	–	–	–
Eq. 3.4	–	21	−10	–	-2×10^{-5}	–	–	–	–
Eq. 3.5	–	−8.8	−11	–	-9×10^{-6}	–	–	–	–
Eq. 3.6	–	42	–	–	–	–	–	–	–
Eq. 2.1	−113	−50	–	−40	–	24.6	–	–	–
Eq. 2.2	−141	−14	−1.7	−76	-6×10^{-5}	24.6	–	440	–
Eq. 2.3	−83	−64	−19	–	-9×10^{-6}	–	17	–	407

[a] ΔH_c (kJ/mol), ΔS_c (J/Kmol), ΔV_c (cm^3/mol), and ΔC_p (J/Kmol), $\Delta\beta$ respectively represent the enthalpy, entropy, volume, heat capacity, and compressibility differences for the crystallization equilibria of Table 1. $W_G^{Di\text{-}En}$ and $W_G^{Di\text{-}CaTs}$ are excess mixing energies for pyroxene components; $W_G^{Si\text{-}Ca}$ and $W_G^{Si\text{-}Na}$ are excess mixing energies for liquid components (kJ/mol). These quantities are from regression coefficients for the equations given in Tables 2 and 3. Typical standard deviations on regression coefficients are as follows: ΔH_c, 27%; ΔS_c, 15%; ΔV_c, 35%; ΔC_p, 39%; $W_G{}^{Si\text{-}Ca}$, 35%; $W_G{}^{Si\text{-}N}$, 10%

with composition, T or P. For example, changes in melt speciation might be expected over the P interval examined (Li et al. 1995), which should affect the activities of liquid components.

Temperature estimation is also a crucial element of igneous petrogenesis. From mineral stoichiometry constraints (Langmuir and Hanson 1981) it is possible to calculate clinopyroxene saturation temperatures using liquid composition information. However, as might be expected from the above discussion, inversion of Eqs. 3.2–3.7 (Table 3), will not be as precise as a direct calibration for the expression $1/T = f(P, X_i^{liq})$. An empirical expression for the prediction of clinopyroxene saturation temperatures is thus presented in Table 3, as Equation 3.8. Using Equation 3.8, clinopyroxene saturation temperatures for the calibration data are recovered with an error 51 K (Fig. 7); this value compares to an error of 89 K when Eqs. 3.2–3.7 are inverted for temperature.

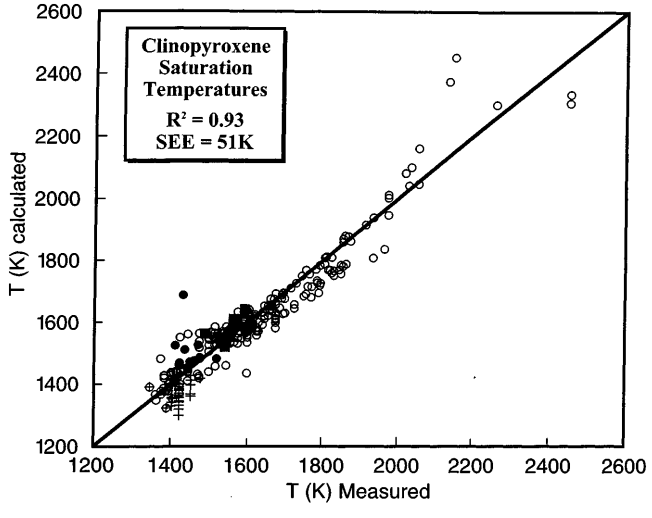

Fig. 7 Equation 3.8 (Table 3) is used to estimate the temperature of clinopyroxene saturation, T^{CpxSat}. Observed Ts are recovered with an error of 50 K for the calibration data. Symbols for the hi-lighted test data are indicated in Fig. 4 caption

Summary

Expressions for clinopyroxene + liquid equilibrium are developed from least-squares analysis of experimental clinopyroxene + liquid pairs. Most variables are based on thermodynamic relationships, but the expressions of Table 3 include empirical terms so that non-linear regression procedures could be avoided. These expressions reliably reproduce clinopyroxene compositions from both calibration and test data sets. The calibration and test data range from 1 atm to 100 kbar and 1300 to 2450 K, and thus the models should be useful for addressing a wide range of geologic problems, with little extrapolation. By focusing upon the prediction of clinopyroxene compositions, this study augments the efforts of Nielsen et al. (1988), Ariskin et al. (1993), and Sack and Ghiorso (1994) as well as greatly expanding upon the P and T ranges of these calibrations. Partition coefficients for Na and Ti were also determined since such expressions are useful in the study of mantle melting. Since Na partitioning is P-sensitive, partial melting depths may be extracted from the calibrated K_d.

By calibrating large data sets, experimental error placed limits upon the amount of fine scale variation that could be resolved by the models, especially for minor components. Future modeling efforts might focus upon the variation of acmite or additional Ti- and Al-bearing components, the effects of f_{O_2}, or data sets that include more silica-rich compositions.

Acknowledgements I thank David Walker for his guidance through this project. I also thank David Walker, John Longhi, Rosamond Kinzler and Charles Langmuir for helpful comments and reviews of the paper, and Paul Asimow for his aid in applying the MELTS program. This paper greatly benefited from comments by Andrei Girnis, Daniel Farber, Heather Bacon-Putirka and reviews by Roger Nielsen, Timothy Grove, Mark Ghiorso, and an anonymous reviewer. UCRL-JC-131481.

References

Adam J, Green TH (1994) The effects of pressure and temperature on the partitioning of Ti, Sr and REE between amphibole, clinopyroxene and basanitic melts. Chem Geol 117: 219–233

Ariskin AA, Frenkel MY, Barmina GS, Nielsen RL (1993) COMAGMAT: a FORTRAN program to model magma differentiation processes. Comp Appl Geosci 19: 1155–1170

Baker MB, Stolper EM (1994) Determining the composition of high-pressure mantle melts using diamond aggregates. Geochim Cosmochim Acta 58: 2811–2827

Bartels KS, Kinzler RJ, Grove TL (1991) High pressure phase relations of primitive high-alumina basalts from Medicine Lake volcano, northern California. Contrib Mineral Petrol 108: 253–270

Bender JF, Langmuir CH, Hanson GN (1984) Petrogenesis of basalt glasses from the Tamayo Region, East Pacific Rise. J Petrol 25: 213–254

Blundy JD, Falloon TJ, Wood BJ, Dalton JA (1995) Sodium partitioning between clinopyroxene and silicate melts. J Geophys Res 100: 15501–15515

Buseck PR, Nord GL, Veblen DR (1980) Subsolidus phenomena in pyroxenes. In: Prewitt CT (ed) Pyroxenes (Reviews of Mineralogy vol. 7): Mineralogical Society of America, Washington DC, pp 117–212

Delano JW (1980) Chemistry and liquidus phase relations of Apollo 15 red glass: implications for the deep lunar interior. Proc Lunar Planet Sci Conf 11: 251–288

Elthon D, Scarfe CM (1984) High-pressure phase equilibria of a high-magnesia basalt and the genesis of primary oceanic basalts. Am Mineral 69: 1–15

Falloon TJ, Green DH (1987) Anhydrous partial melting of MORB pyrolite and other peridotite compositions at 10 kbar: implications for the origin of primitive MORB glasses. Mineral Petrol 37: 181–219

Forsythe LM, Nielsen RL, Fisk MR (1994) High-field-strength element partitioning between pyroxene and basaltic to dacitic magmas. Chem Geol 117: 107–125

Gee LL, Sack R (1988) Experimental petrology of melilite nephelinites. J Petrol 29: 1233–1255

Ghiorso MS, Sack RO (1995) Chemical mass transfer in magmatic processes IV. A revised and internally consistent thermodynamic model for the interpolation and extrapolation of liquid-solid equilibria in magmatic systems at elevated temperatures and pressures. Contrib Mineral Petrol 119: 197–212.

Grove TL, Juster TC (1989) Experimental investigations of low-Ca pyroxene stability and olivine-pyroxene-liquid equilibria at 1-atm in natural basaltic and andesitic liquids. Contrib Mineral Petrol 103: 287–305

Grove TL, Kinzler RJ, Bryan WB (1992) Fractionation of mid-ocean ridge basalt (MORB). Geophys Monogr Am Geophys Union 17: 281–310

Grover JE (1980) Thermodynamics of pyroxenes. In: Prewitt CT (ed) Pyroxenes (Reviews of Mineralogy vol. 7). Mineralogical Society of America, Washington DC, pp 341–418

Grover JE, Orville PM (1969) The partitioning of cations between coexisting single- and multi-site phases with application to the assemblages: orthopyroxene-clinopyroxene and orthopyroxene-olivine Geochim Cosmochim Acta 33: 205–226

Hack PJ, Nielsen RL, Johnston AD (1994) Experimentally determined rare-earth element and Y partitioning behavior between clinopyroxene and basaltic liquids at pressures up to 20 kbar. Chem Geol 117: 89–105

Hauri EH, Wagner TP, Grove TL (1994) Experimental and natural partitioning of Th, U, Pb and other trace elements between garnet, clinopyroxene and basaltic melts. Chem Geol 117: 149–166

Jefferys WH, Berger JO (1992) Ockam's Razor and Baysian analysis. Am Sci 80: 64–72

Juster TC, Grove TL, Perfit MR (1989) Experimental constraints on the generation of FeTi basalts, andesites and rhyodacites at the Galapagos Spreading center, 85°W and 95°W. J Geophys Res 94: 9251–9274

Kinzler RJ (1997) Melting of mantle peridotite at pressures approaching the spinel to garnet transition: application to mid-ocean ridge basalt petrogenesis. J Geophys Res 102: 853–874

Kinzler RJ, Grove TL (1992) Primary magmas of mid-ocean ridge basalts 1. Experiments and methods. J Geophys Res 97: 6885–6906

Lange RA, Carmichael ISE (1987) Densities of Na_2O-K_2O-CaO-MgO-FeO-Fe_2O_3-Al_2O_3-TiO_2-SiO_2 liquids: new measurements and derived partial molar properties. Geochim Cosmochim Acta 51: 2931–2946

Langmuir CH, Hanson GN (1981) Calculating mineral-melt equilibria with stoichiometry, mass balance, and single component distribution coefficients. In: Newton RC, Navrotsky A, Wood BJ (eds) Thermodynamics of minerals and melts (Advances in Physical Geochemistry vol. 1). Springer, Berlin Heidelberg New York, pp 247–271

Langmuir CH, Klein EM, Plank T (1992) Petrological systematics of mid-ocean ridge basalts: constraints on melt generation beneath ocean ridges. Geophys Monogr Am Geophys Union 71: 183–280

Li D, Secco RA, Bancroft GM, Fleet ME (1995) Pressure induced coordination change of Al in silicate melts from Al K edge XANES of high pressure $NaAlSi_2O_6$-$NaAlSi_3O_8$ glasses. Geophys Res Lett 22: 3111–3114

Lindsley DH (1980) Phase equilibria of pyroxenes at pressures >1 atmosphere. In: Prewitt CT (ed) Pyroxenes (Reviews of Mineralogy vol. 7). Mineralogical Society of America, Washington DC, pp 289–308

Lindsley DH (1983) Pyroxene thermometry. Am Mineral 68: 477–493

Longhi J (1995) Liquidus equilibria of some primary lunar and terrestrial melts in the garnet stability field. Geochim Cosmochim Acta 59: 2375–2386

Longhi J (1996) Investigation of the origin of hi-Ti basalts by polybaric fractional fusion. Lunar and Planet Sci Conf XVII, Lunar and Planet Inst, Houston pp 767–768

Longhi J, Bertka CM (1996) Graphical analysis of pigeonite-augite liquidus equilibria. Am Mineral 81: 685–695

Longhi J, Pan V (1988) A reconnaisance study of phase boundaries in low-alkali basaltic liquids. J Petrol 29: 115–147

Navrotsky A (1981) Thermodynamics of mixing in silicate glasses and melts. In: Newton RC, Navrotsky A, Wood BJ (eds) Thermodynamics of minerals and melts. Springer, Berlin Heidelberg, New York, pp 189–206

Navrotsky A, Ziegler D, Oestrike R, Maninar P (1989) Calorimetry of silicate melts at 1773 K: measurement of enthalpies of fusion and of mixing in the systems diopside-anorthite-albite and anorthite-forsterite. Contrib Mineral Petrol 101: 122–130.

Nielsen RL, Drake MJ (1979) Pyroxene-melt equilibria. Geochim Cosmochim Acta 43: 1259–1272

Nielsen RL, Davidson PM, Grove TL (1988) Pyroxene-melt equilibria: an update model. Contrib Mineral Petrol 100: 361–373

Nordstrom DK, Munoz JL (1986) Geochemical thermodynamics. Blackwell Sci Publ, Brookline, MA

Ottonello G (1992) Interactions and mixing properties in the (C2/c) clinopyroxene quadrilateral. Contrib Mineral Petrol 111: 53–60

Putirka K (1998) Garnet + liquid equilibrium. Contrib Mineral Petrol 131: 273–288

Putirka K, Johnson M, Kinzler R, Longhi J, Walker D (1996) Thermobarometry of mafic igneous rocks based on clinopyroxene-liquid equilibria, 0–30 kbar. Contrib Mineral Petrol 123: 92–108

Ratkowsky DA (1990) Handbook of non-linear regression models. Marcel Decker Inc., New York

Ray GL, Shimuzu N, Hart SR (1983) An ion microprobe study of the partitioning of trace elements between clinopyroxene and liquid in the system diopside-albite-anorthite. Geochim Cosmochim Acta 47: 2131–2140

Richet P, Bottinga Y (1986) Thermochemical properties of silicate glasses and liquids: a review. Rev Geophys 24: 1–25

Robie RA, Hemingway BS, Fisher JR (1979) Thermodynamic properties of minerals and related substances at 298.15 K and 1 bar (10^5 Pascals) pressure and at higher temperatures. US Geol Surv Bull 1452: 456

Robinson JAC, Wood BJ, Blundy JD (1998) The beginning of melting of fertile and depleted peridotite at 1.5 GPa. Earth Planet Sci Lett 155: 97–111

Roeder PL, Emslie RF (1970) Olivine-liquid equilibrium. Contrib Mineral Petrol 29: 275–289

Ryan TP (1997) Modern regression methods. Wiley, New York

Sack RO, Ghiorso MS (1994) Thermodynamics of multicomponent pyroxenes: III. Calibration of $Fe^{2+}(Mg)_{-1}$, $TiAl_2(MgSi_2)_{-1}$, $TiFe_2^{+3}(MgSi_2)_{-1}$, $AlFe^{+3}(MgSi)_{-1}$, $NaAl(CaMg)_{-1}$, $Al_2(MgSi)_{-1}$, and $Ca(Mg)_{-1}$ exchange reactions between pyroxenes and silicate melts. Contrib Mineral Petrol 118: 271–296

Sack RO, Walker D, Carmichael ISE (1987) Experimental petrology of alkalic lavas: constraints on cotectics of multiple saturation in natural basic liquids. Contrib Mineral Petrol 96: 1–23

Skulski T, Minarik W, Watson EB (1994) High-pressure experimental trace-element partitioning between clinopyroxene and basaltic melts. Chem Geol 117: 127–147

Takahashi E (1986) Melting of a dry peridotite KLB-1 up to 14 GPa: implications on the origin of peridotitic upper mantle. J Geophys Res 91: 9367–9382

Tormey DR, Grove TL, Bryan WB (1987) Experimental petrology of normal MORB near the Kane Fracture Zone: 22°–25° N, mid-Atlantic Ridge. Contrib Mineral Petrol 96: 121–139

Walter MJ, Presnall DC (1994) Melting behavior of simplified lherzolite in the system CaO-MgO-Al_2O_3-SiO_2-Na_2O from 7 to 35 kbar. J Petrol 35: 329–359

Wei K, Tronnes RG, Scarfe CM (1990) Phase relations of aluminum-undepleted and aluminum-depleted komatiites at pressures of 4–12 GPa. J Geophys Res 95: 15817–15827

Yasuda A, Fujii T (1994) Melting phase relations of an anhydrous mid-ocean ridge basalt from 3 to 20 GPa: implications for the behavior of subducted oceanic crust in the mantle. J Geophys Res 99: 9401–9414